Hindawi
International Journal of Aerospace Engineering
Volume 2019, Article ID 2918646, 19 pages
https://doi.org/10.1155/2019/2918646

Research Article

Research on Simulation and Performance Optimization of Mach 4 Civil Aircraft Propulsion Concept

Min Chen,[1] **Zihao Jia**,[1] **Hailong Tang**,[1] **Yi Xiao**,[2] **Yonghang Yang**,[3] **and Feijia Yin**[4]

[1]*School of Energy and Power Engineering, Beihang University, Beijing 100191, China*
[2]*Aero Engine Academy of China, Beijing 101304, China*
[3]*AECC Sichuan Gas Turbine Research Establishment, Sichuan 610500, China*
[4]*Delft University of Technology, 2629HS Delft, Netherlands*

Correspondence should be addressed to Hailong Tang; 75249612@qq.com

Received 8 May 2018; Accepted 24 September 2018; Published 14 January 2019

Guest Editor: Konstantinos Kyprianidis

Supersonic civil aircraft is of a promising area in the development of future civil transport, and aircraft propulsion system is one of the key issues which determine the success of the aircraft. To get a good conceptual design and performance investigation of the supersonic civil aircraft engine, in this article, a fast, versatile as well as trust-worthy numerical simulation platform was established to analyze the Mach 4 turbine-based combined cycle (TBCC) engine concept so as to be applied to the supersonic civil aircraft. First, a quick and accurate task requirement analysis module was newly established to analyze the mission requirement of the Mach 4 supersonic civil aircraft. Second, the TBCC engine performance simulation model was briefly presented and the number of engines on the supersonic civil aircraft was analyzed, considering single engine inoperative. Third, the Stone model and the DLR method were investigated to estimate the engine jet noise and the NO_x emission of the Mach 4 supersonic civil aircraft. Finally, a multiobjective optimization tool made up of a response surface method and a genetic algorithm was developed to optimize the design parameters and the control law of the TBCC engine, in order to make the Mach 4 supersonic civil aircraft engine with better performance, lower noise, and lower emissions. The uniqueness of the developed analysis tool lies in that it affords a numerical simulation platform capable of investigating the task requirement analysis module of the supersonic civil aircraft, engine jet noise prediction model, and the NO_x emission prediction model, as well as a multiobjective performance optimization tool, which is beneficial for the conceptual design and performance research of Mach 4 supersonic civil aircraft's propulsion system.

1. Introduction

Supersonic civil aircraft with higher speed can offer significant time savings in the long-range flight compared with the subsonic one. With the stop of the Concorde operation since 2003, the first generation of the supersonic civil aircraft has become a history. However, as the international communication is becoming more and more frequent, the long-range and short-time flight has a promising market potential. Research has shown that the supersonic civil aircraft could capture up to seventy percent of the long-haul markets in cases where it can offer significant time savings over a long-range subsonic aircraft [1]. For the broad market prospect, many aviation powers began to develop the supersonic civil aircraft. For example, America proposed the plan for high-speed civil transport aircraft, such as the supersonic transport (SST) and high-speed research (HSR) [2]. Europe put the first supersonic commercial aircraft into operation, which was stopped in 2003 due to the factors of safety consideration, economy, and noise problem, but it achieved in getting experience of the development in the supersonic aircraft production and the market operation. After that, a Long-Term Advanced Propulsion Concepts and Technologies (LAPCAT) program has been advanced for the supersonic passenger aircraft in Europe since 2005. Russia and Japan are also interested in the development of the supersonic civil aircraft, such as Russian T244, T344 development plans, Japanese National Experimental

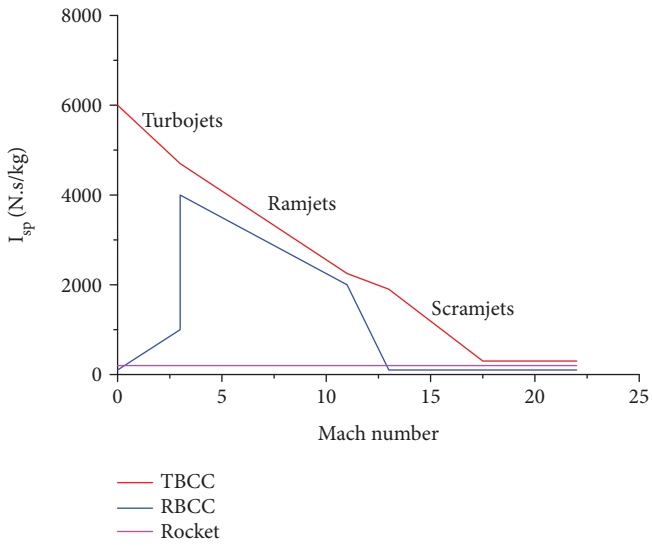

Figure 1: Specific impulse comparison between different propulsion types with Mach number variation [3].

Supersonic Transport (NEXST), and hypersonic transport propulsion system research (HYPR) plans.

Because the supersonic vehicles have a wide flight Mach range, the propulsion technology is one of the most important challenges in the process of meeting the flight mission requirement. Figure 1 shows the specific impulse (I_{sp}) comparison between different propulsion types with Mach number variation [3], where RBCC means a rocket-based combined cycle and specific impulse (I_{sp}) means the thrust produced by the unit mass of propellant. From the chart, it is known that when the Mach number is from 0 to 3, the turbine engine has the highest specific impulse. When the Mach number varies from 3 to a higher level, the ramjet engine has the highest specific impulse. Since the supersonic civil aircraft has to operate from take-off to Mach number 5, the TBCC engine is one of the most optimal engine types, combined of the turbofan engine and the ramjet engine. Then, Figure 2 shows two typical TBCC engine configurations. Among these, the parallel type has independent engine operating modes due to the separate gas paths, greater windward area, and volume. In contrast with the parallel type, the tandem type has the advantages of more compact structure, lighter quality, and more complicated matching of aerodynamic performance to satisfy the wide flight range. Thus, this article selects the tandem-type TBCC engine (Figure 2(b)) as the research object.

A variety of new generation supersonic civil aircraft concepts have been put forward in some literatures [4–21], for example, the conceptual design of Mach 5 TBCC engine which is applied into the supersonic civil aircraft has been investigated [22]. However, for Mach 5 TBCC engine, the inlet adjustment is more complicated, and the total inlet temperature can reach around 1300 K. So, it is more challenging to solve the airframe thermal protection problem based on the existing material and technology, due to the high stagnant temperature due to extremely high Mach. Meanwhile, the engine matching problem with the inlet and exhaust system under a wide flight Mach range also causes great troubles. Apart from these, assuming that the flight mission profile [22] is the same, with the increase of the Mach number, the time savings gradually decrease as shown in Figure 3. For example, the distance of the trans-Pacific flight from Shanghai to New York is about 13,800 km. According to Figure 3, the journey time for the Mach 5 supersonic civil aircraft is only about half an hour less than Mach 4. Thus, considering the above factors and referring to the requirements of the aircraft designers, in this article, the cruise Mach number of the supersonic civil aircraft is changed from Mach 5 to Mach 4.

In this article, a fast, versatile, and trustworthy numerical simulation platform has been established to analyze the Mach 4 TBCC engine concept for the supersonic civil aircraft, which includes the newly developed task requirement analysis module of the supersonic civil aircraft, engine jet noise, and the NO_x emission prediction models, as well as a multiobjective optimization tool based on the response surface methodology. Firstly, Section 2 establishes the calculation module, which is used to analyze the mission requirement of the Mach 4 supersonic civil aircraft. Then, Section 3 presents the TBCC engine performance simulation module briefly and analyzes the number of engines for the supersonic civil aircraft, considering single engine inoperative. The two following sections conduct studies on the quick and trusted prediction models used to estimate the engine jet noise and the NO_x emission of the supersonic civil aircraft. Section 6 proposes the multiobjective optimization tool to optimize the design parameters and control laws of the TBCC engine, in order to make the Mach 4 supersonic civil aircraft engine with better performance, lower noise, and lower emissions.

2. Task Requirement Analysis of the Mach 4 Supersonic Civil Aircraft

To put the concept design of the next generation supersonic civil aircraft and its propulsion system into practise, the mission requirement is essential, such as the cruise speed, the flight range, and the passenger capacity. To meet the major long-distance travel market requirement in China and to demonstrate the superior performance in time saving, trans-Pacific (from mainland China to United States West Coast), relative short-travelling-time (less than 4 hours) flight is of requirement. This mission requirement emphasizes that the range should be above 10,000 km according to the range survey in Figure 4.

For all the aircraft concepts, economy is one of the most important factors that must be considered into the preliminary design stage. So, we use the fuel efficiency figure of merit (FOM) to evaluate the economy and define FOM as follows.

$$\mathrm{FOM} = \frac{\mathrm{PAX} \cdot R}{W_{\mathrm{Fblock}}}, \tag{1}$$

where PAX means passenger number, R means range, and W_{Fblock} means block fuel weight.

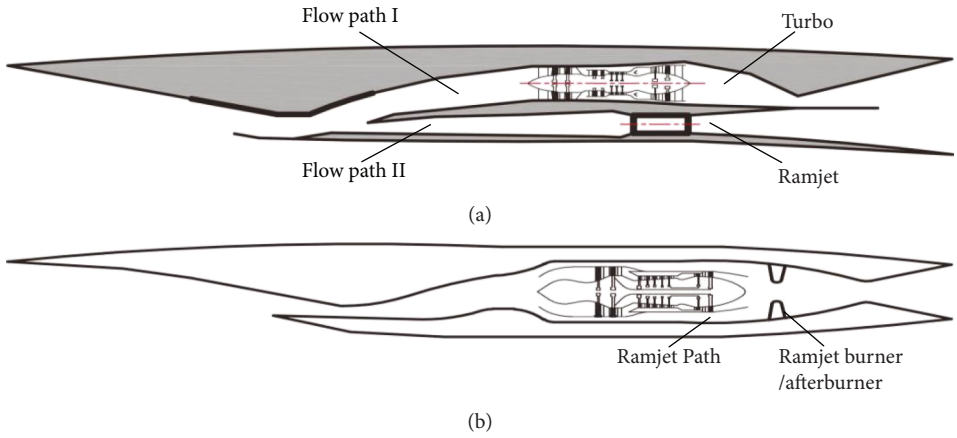

Figure 2: Two typical TBCC engine configurations ((a) parallel type; (b) tandem type).

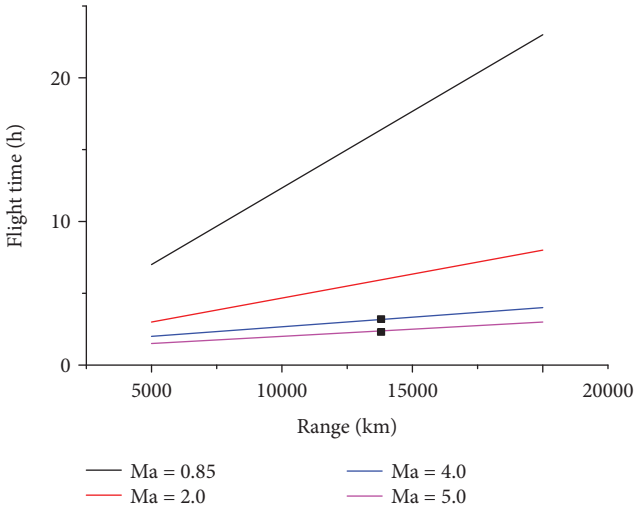

Figure 3: The flight time contrast at different speeds.

Another important factor which must be considered in the preliminary design stage is take-off gross weight (W_{TO}), because it is relative to the requirement of the propulsion system and can also meet the demand of an airport.

However, in the previous investigations of the new generation supersonic civil aircraft, such as the 250-passenger, Mach 4 high-speed civil transport [4], influence that details of some important input parameters on FOM and W_{TO} are not given, and these important parameters include flight range (R) and PAX, two technical parameters—cruise lift-to-drag ratio (L/D) and cruise specific fuel consumption (SFC). So, this section will analyze the influences of the important parameters on FOM and W_{TO}, in order to analyze the task requirements of the Mach 4 supersonic civil aircraft. The published research data of the related supersonic civil aircraft are summarized in Table 1 [1, 3–5].

2.1. Aircraft Preliminary Weight Estimation Method. In order to analyze the parameter FOM which is related to W_{Fblock} and W_{TO}, we propose a preliminary aircraft weight estimation method.

Generally, W_{TO} consists of payload (W_{PL}) and total fuel weight (W_F) which includes W_{Fblock} and reserve fuel weight ($W_{Freserve}$), as well as operating empty weight (W_{OE}), shown as follows.

$$W_{TO} = W_{PL} + W_F + W_{OE}. \quad (2)$$

It can be rewritten as follows.

$$W_{TO} = \frac{W_{PL}}{1 - W_F/W_{TO} - W_{OE}/W_{TO}}. \quad (3)$$

In 3, W_F/W_{TO} means fuel weight coefficient, which is replaced by mf. W_{OE}/W_{TO} with the meaning of the operating empty weight coefficient is replaced by moe. Details of payload, total fuel weight, and operating empty weight estimation are presented as below.

2.1.1. Payload (W_{PL}). Weight of each passenger including baggage is assumed to be 98 kg according to the existing research of the related supersonic civil aircraft in Table 1 [1, 3–5]. If PAX is given, W_{PL} can be calculated by using the following equation.

$$W_{PL} = 98 \times \text{PAX}. \quad (4)$$

2.1.2. Total Fuel Weight (W_F). Accurate estimation method of total fuel weight needs to split the flight profiles into many small sections, then integrate the fuel consumption of each section. However, this estimation method needs unavailable parameters of the aircraft and propulsion system at different flight conditions.

In order to estimate W_F quickly, it is divided into two parts—W_{Fblock} and $W_{Freserve}$.

For W_{Fblock}, the flight mission profiles are segmented into 7 sections [23]: engine start and warm-up, taxi out, take-off, climb, cruise, descent, and taxi in. Ratio of aircraft weight (ROW$_i$) ($i = 1, 2, 3, 4, 5, 6, 7$) is defined as ROW$_i$ = W_i/W_{i-1}, where W_i is the aircraft weight at the ending of one section, W_{i-1} is the one at the start of this section, and W_0 is W_{TO}. For the 5th section, the ratio of cruise section is

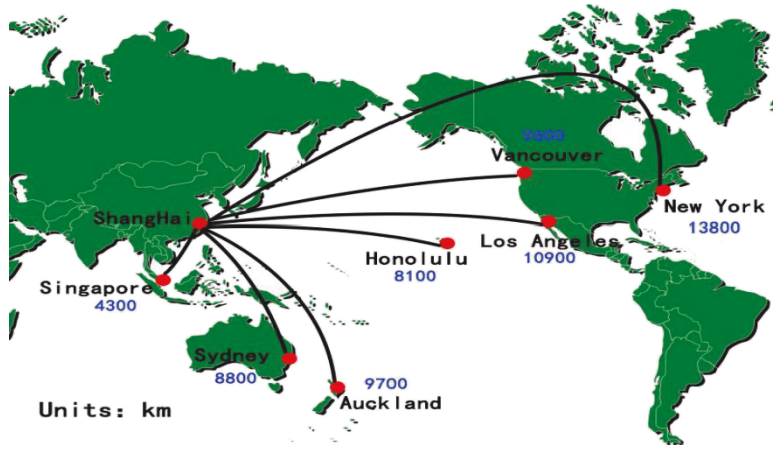

Figure 4: Range survey.

Table 1: Data survey of the concept scheme of the supersonic civil aircraft [1, 3–5, 18, 19].

	Ma	R (km)	PAX	W_{TO} (kg)	W_{PL} (kg)	W_{OE} (kg)	W_F (kg)	W_{PL}/PAX (kg)	FOM (PAX·km/kg)
Mach 3	3.0	12,038	250	323,727	24,864	123,822	175,043	99	19.9
Mach 4	4.0	12,038	251	392,656	24,963	138,678	229,015	99	14.9
HSCT BOE MFTF5093	2.4	9260	300	320,051	29,433	124,141	166,477	98	18.8
HSCT BOE ACE701510	2.4	9260	300	323,914	29,434	123,918	170,562	98	18.5

Table 2: Values of relevant parameters for calculating W_F [1, 3–5].

$\frac{R_{nc}}{R}$	$\frac{R_c}{R}$	ROW_{nc}	$\frac{W_{Freserve}}{W_{TO}}$
9.36%	90.64%	0.8584	6.51%

also written as ROW_c. Then, the proportion of W_{Fblock} devoted to W_{TO} is shown as follows.

$$\frac{W_{Fblock}}{W_{TO}} = 1 - \prod_{i=1}^{i=7} ROW_i. \quad (5)$$

ROW_c can be gotten through Breguet range equation shown as follows.

$$R_c = \frac{V_0}{g\,SFC}\frac{L}{D}\ln\left(\frac{W_{start}}{W_{end}}\right) = \frac{V_0}{g\,SFC}\frac{L}{D}\ln\left(\frac{1}{ROW_c}\right), \quad (6)$$

where R_c is the range of the cruise section (km), g is gravity constant (m/s^2), L/D is the cruise lift-to-drag ratio, SFC is cruise specific fuel consumption (kg/h/N), V_0 is cruise velocity (km/h), W_{start} is aircraft weight at the start of the cruise section, and W_{end} is aircraft weight at the end of the cruise section. And the relevant parameters for calculating W_F are listed in Table 2. For long-range flight, noncruise range (R_{nc}) occupies 9.36% of the total range according to one investigated supersonic civil aircraft concept [3] and then R_c is 90.64% of the total range (R).

For the noncruise sections, we multiply each noncruise section's ROW_i written as ROW_{nc}, as follows.

$$ROW_{nc} = ROW_1 \times ROW_2 \times ROW_3 \times ROW_4 \times ROW_5 \times ROW_6 \times ROW_7. \quad (7)$$

ROW_{nc} is a given value referring to the relevant research of the supersonic civil aircraft [3]. So W_{Fblock} can be got by allying (5)~(7). For $W_{Freserve}$, it is 6.51% of W_{TO} which is given according to the statistical data of the supersonic civil aircraft [1, 3–5].

So, fuel weight coefficient mf can be calculated as follows.

$$\begin{aligned} mf = \frac{W_F}{W_{TO}} &= \frac{W_{Fblock}}{W_{TO}} + \frac{W_{Freserve}}{W_{TO}} \\ &= \left(1 - \prod_{i=1}^{i=7} ROW_i\right) + \frac{W_{Freserve}}{W_{TO}} \\ &= (1 - ROW_c + ROW_{nc}) + 0.0651. \end{aligned} \quad (8)$$

Thus, W_F can be calculated as follows:

$$W_F = mf \times W_{TO}. \quad (9)$$

2.1.3. Operating Empty Weight (W_{OE}). W_{OE} is commonly got by building the relation with W_{TO} [23, 24]. According to the existing research data of the related supersonic civil aircraft in Table 1 [1, 3–5], the fitted relation is shown in Figure 5.

So, W_{OE} can be calculated as follows.

$$W_{OE} = moe \times W_{TO}, \quad (10)$$

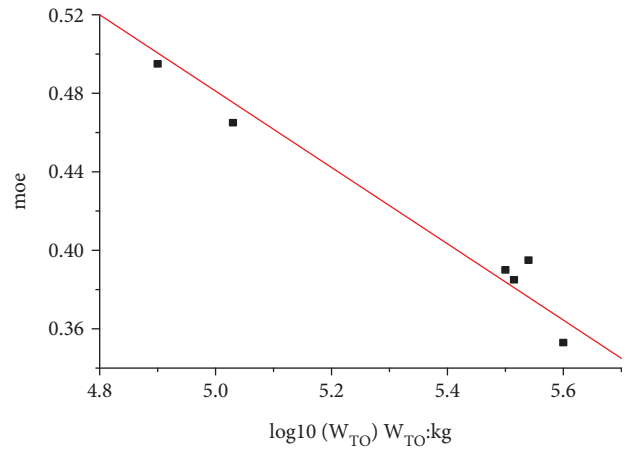

FIGURE 5: The relation between moe and W_{TO} of the supersonic civil aircraft.

where moe signifies operating empty weight coefficient. The whole process of aircraft preliminary weight estimation is shown in Figure 6, which involves an iteration process.

2.2. The Influence Analysis of PAX and SFC on FOM and W_{TO}. Based on the related supersonic civil aircraft investigation [10], the Mach 4 supersonic reference cruise L/D is 7.79. Moreover, according to the existing research of the TBCC engine [22], Mach 4 TBCC engine reference cruise SFC is 2.00 kg/h/daN. By using the introduced aircraft preliminary weight estimation method and definition of FOM, influence of PAX and R on FOM and W_{TO} is shown in Figure 7.

From the above figure, if R keeps invariant, increasing PAX makes both FOM and W_{TO} increase directly. According to the definition of FOM, it will be influenced by R, PAX, and W_{Fblock}. Increase of PAX makes both FOM and W_{Fblock} increase immediately. But the increase of W_{Fblock} results in the decrease of FOM. However, the effect of PAX outweighs the opposite effect of W_{Fblock} on FOM. Thus, in fact FOM is rising with the increase of PAX.

If PAX keeps constant, the increase of R makes FOM reduce and W_{TO} increase, because the increase of R naturally makes W_F and W_{OE} increase, thus making W_{TO} growing. Incremental R makes W_{Fblock} increase therefore makes FO M decrease. According to Figure 7, both R and PAX have severe influences on FOM and W_{TO}.

Because aircraft cruise L/D and propulsion system cruise SFC represent the technical level of the aircraft and engine. The influences of the aircraft cruise L/D and engine cruise S FC on FOM and W_{TO} should also be analyzed. The reference concept (R = 10,000 km, PAX = 300) should be treated as the research object. While in the reference concept, influences of cruise L/D and cruise SFC on FOM and W_{TO} are shown in Figure 8.

As shown in Figure 8(a), when cruise SFC keeps constant, increasing cruise L/D makes FOM increase and W_{TO} decrease, vice versa. While on shown in Figure 8(b), if cruise L/D keeps constant, SFC reduction makes FOM increase and W_{TO} reduce, vice versa. Both cruise L/D and cruise SFC have significant influence on FOM and W_{TO}. Based on preceding analysis, improving cruise L/D and reducing cruise SFC are an effective method in reducing supersonic civil aircraft weight and improving the economy.

2.3. Sensitivity Analysis of Uncertain Variables on FOM and W_{TO}. In the above shown aircraft preliminary weight estimation method, the noncruise ratio of aircraft weight (ROW_{nc}) and the ratio of noncruise to total range (R_{nc}/R) are given as constant values, where ROW_{nc} is 85.84% and R_{nc}/R is 9.36%. However, ROW_{nc} and R_{nc}/R of different aircraft with different climbing and descent strategies are in a changing state. Thus, it is necessary to make sensitivity analysis of uncertain variables on FOM and W_{TO}.

Let reference concept (PAX = 300, R = 10,000 km, cruise L/D = 7.79, cruise SFC = 2.00 kg/h/daN, ROW_{nc} = 85.84%, and R_{nc}/R = 9.36%) be a benchmark, the influences of RO W_{nc} and R_{nc}/R on FOM and W_{TO} are analyzed as shown in Figure 9.

From the figure, it can be seen that ROW_{nc} has a great influence on both FOM and W_{TO}. For example, −1% change of ROW_{nc} makes FOM −4% and W_{TO} +3%. R_{nc}/R also has certain influence on FOM and W_{TO} but not as prominent as ROW_{nc}. For example, +1% of R_{nc}/R makes FOM about +0.2% and W_{TO} about −0.2%. Although ROW_{nc} and R_{nc}/R have influence on absolute calculation results, they do not affect the trend of FOM and W_{TO} resulting from the variation of PAX, R, cruise L/D, and cruise SFC. In the future in-depth investigation, accurate values of ROW_{nc} and R_{nc}/R are needed to make the result more precise.

Thus, to get a supersonic civil aircraft concept for trans-Pacific and relative short-travelling-time flight, R and PAX are recommended to be 10,000 km and 300 persons, respectively, which makes FOM 14.8 PAX·km/kg and W_{TO} 407 tons.

3. Engine Performance Simulation Model and Selection of the Engine Number considering Single Engine Inoperative

3.1. TBCC Engine Performance Simulation Module. This section describes the performance simulation model of the TBCC engine on the Mach 4 supersonic civil aircraft [22]. A zero-dimensional (0D) variable cycle TBCC engine model controlled by multiple variables is developed to provide a platform suitable for parametric cycle analysis, performance cycle analysis, control law study of the turbofan mode, the ramjet mode, and turbofan/ramjet mode transition. The engine model is viewed as a set of interconnected gas components, whose performance is described in terms of characteristic maps or empirical formulas. And the specific configuration of the TBCC engine is shown as the tandem type (Figure 2(b)). The gas components are coupled together through the balance relationships that are summarized as below.

(1) Power-balance equation for each rotor with the rotor inertia term (turbine power = compressor power + parasitic power + acceleration power)

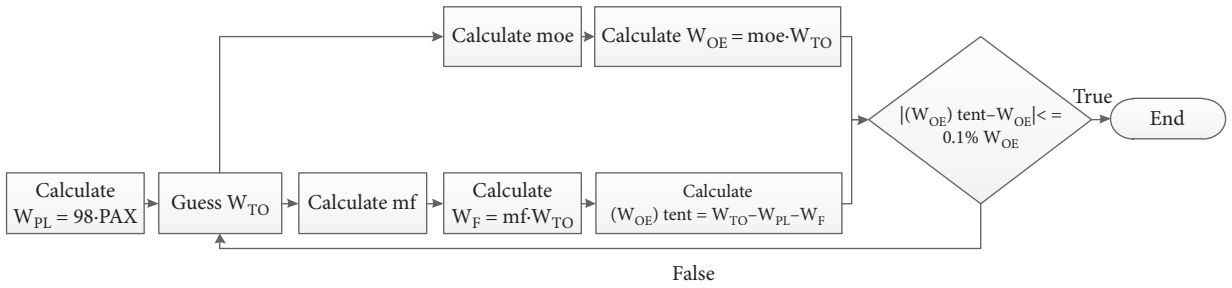

Figure 6: Aircraft preliminary weight estimation flow chart.

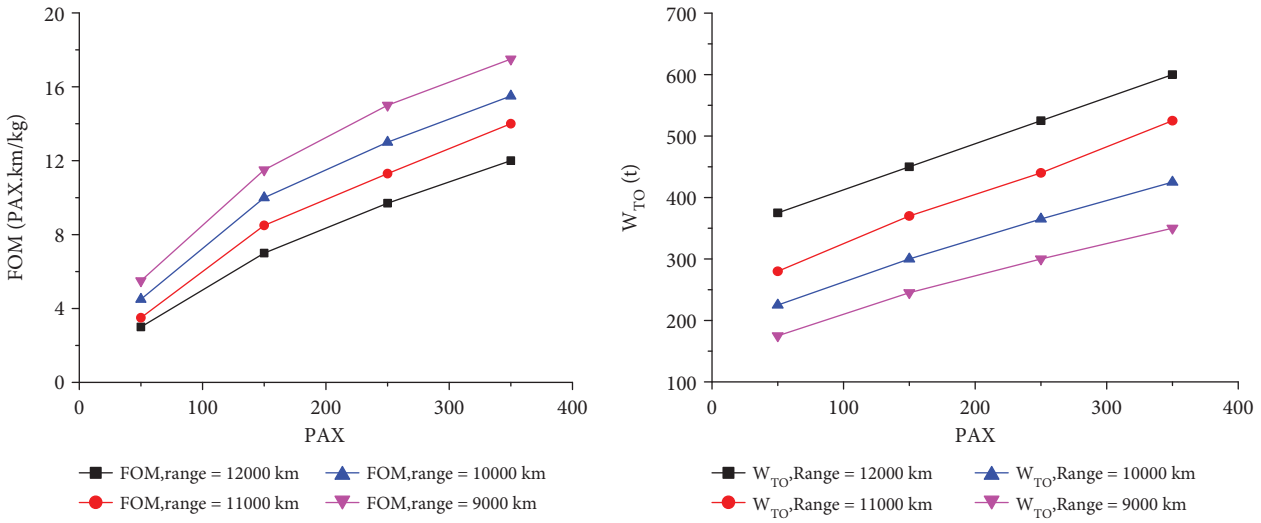

Figure 7: Influence of R and PAX on FOM and W_{TO}.

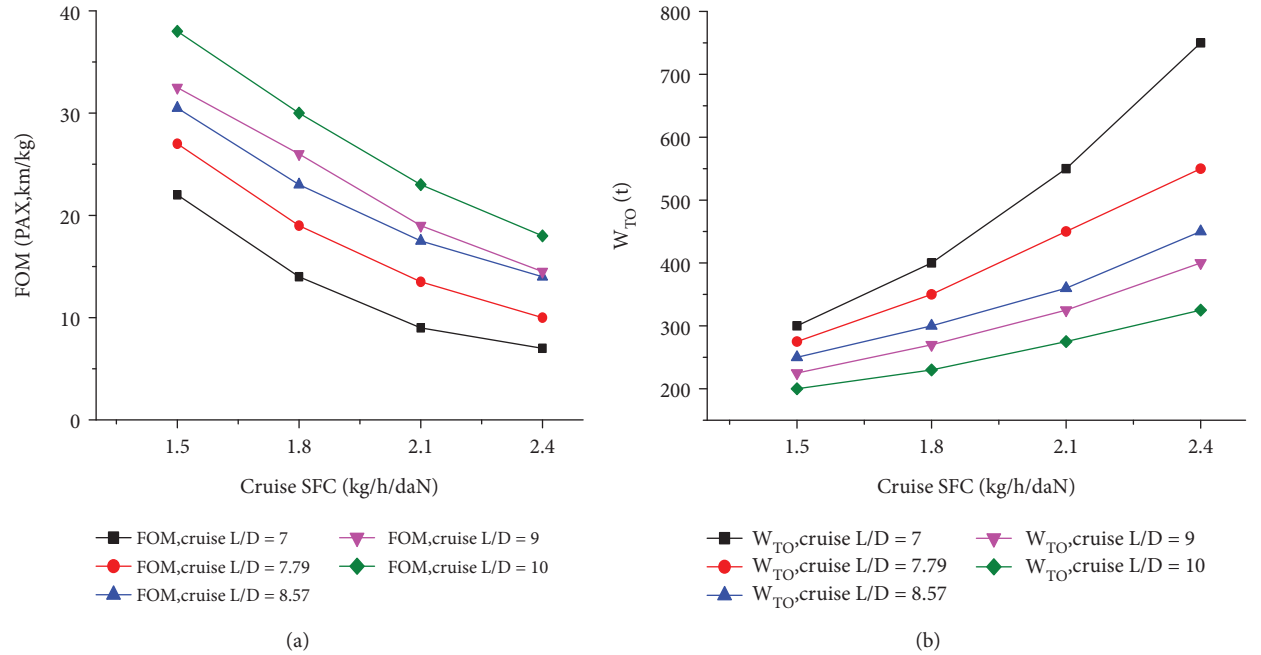

Figure 8: Influences of cruise L/D and cruise SFC on FOM and W_{TO}.

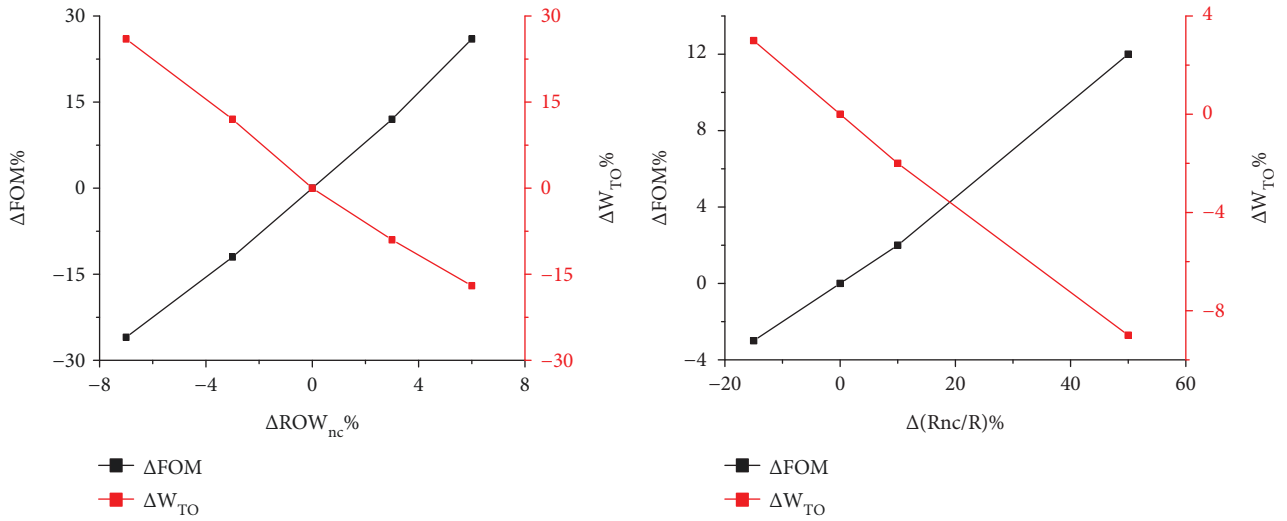

Figure 9: Sensitivity analysis of ROW_{nc} and R_{nc}/R.

(2) Flow compatibility between the connected gas components

(3) Assurance of static pressure balance at the mixing surface boundary of the duct and core flows

Then, a multidimensional Newton Raphson iteration technique was employed to simultaneously satisfy all the balance relation functions to achieve cycle balance at each operation point. Other important features of the engine module are shown below.

(1) Component characteristics of the fan, high pressure compressor (HPCP), low pressure turbine (LPTB), and RJAB were proved by the rig tests [1, 2, 25, 26]

(2) The characteristics of the inlet and nozzle are acquired through the analytical design method, which will be discussed later

(3) Gas property differences, caused by the variation of the gas ingredients, ambient temperature, and ambient humidity, were considered

(4) Other factors were also taken into account, such as the effect of altitude, Mach number, extraction and return of cooling air, and power set aside for aircraft accessories

(5) Combined operation performance of the five variable geometries can be simulated

Finally, the fidelity of this module has been evaluated by the published reference and it is able to meet the requirements of the TBCC engine concept design.

3.2. Selection of the Engine Number considering Single Engine Inoperative. This section calculates the number of engines for the Mach 4 supersonic civil aircraft, considering single engine inoperative. For the existing subsonic aircraft, the engine performance in the take-off and climbing state is extremely important. However, for the supersonic civil aircraft, the thrust requirement in the Mach 4 supersonic cruising state must be satisfied; otherwise, it will decelerate and descend. Thus, if one aircraft engine is inoperative in the cruising state, it will be required to find the right number of engine to land in an alternate airport.

To simplify the research process, the following assumptions are made before the study:

(1) A single engine inoperative occurs at cruising condition (23 km, Ma 4)

(2) Within the range of 0.05 reduction of the flight Mach, the deceleration and the fuel flow remain unchanged

(3) During the aircraft deceleration process, lift = gravity $(\mathrm{Cl} \times (1/2\rho \times V^2) \times A = W \times g)$, where $A = 356.31\ \mathrm{m}^2$ (calculated by the cruising lift = gravity) remains the same

(4) When the difference between the engine thrust and the required aircraft thrust is less than 1 N, the iteration is considered to be completed

Figure 10 shows the flow chart of the algorithm for single engine inoperative process analysis, where the lift coefficient and the lift to drag ratio need to be checked on the Mach altitude characteristic diagram.

According to Figure 11, it can be seen that the abscissa values of the intersection are both more than 3, which means the Mach 4 aircraft can resume cruising condition with one engine inoperable, before the TBCC engines back to the turbofan mode. Meanwhile, the difference of iteration step has limited influence (around 0.5%) on the computational accuracy for the abscissa values (Mach number), and $\Delta\mathrm{Ma} = 0.05$ can reduce iterations. So, $\Delta\mathrm{Ma} = 0.05$ is chosen as the iteration step size.

The following figures present the analysis and comparison of double, three, and four engine schemes under single inoperative process. The different engine configurations lead to the different aircraft weights and demanding thrusts. From Figure 12, it can be seen that when the scheme with double

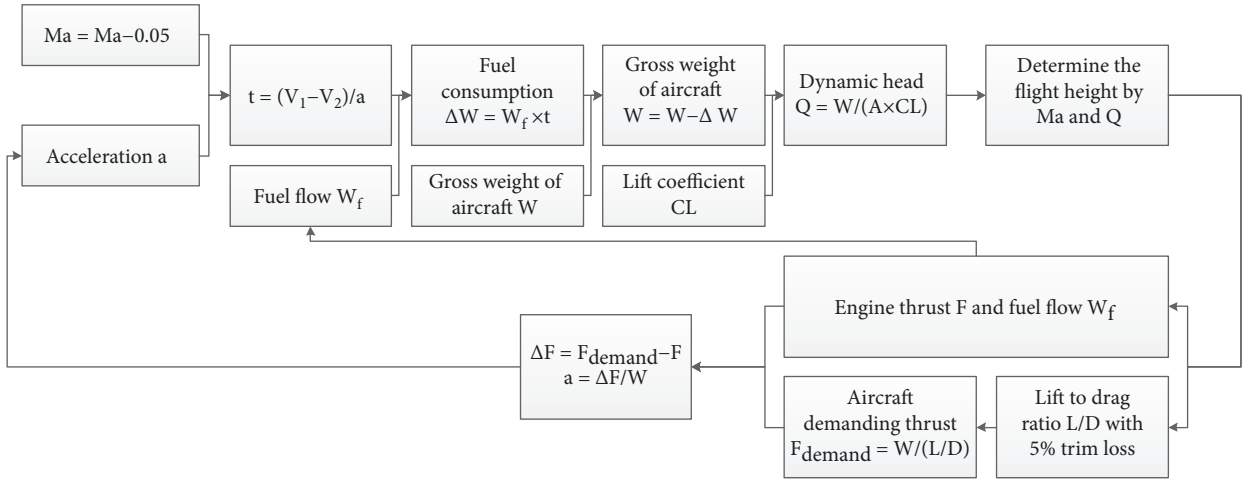

Figure 10: Single engine inoperative analysis flow chart.

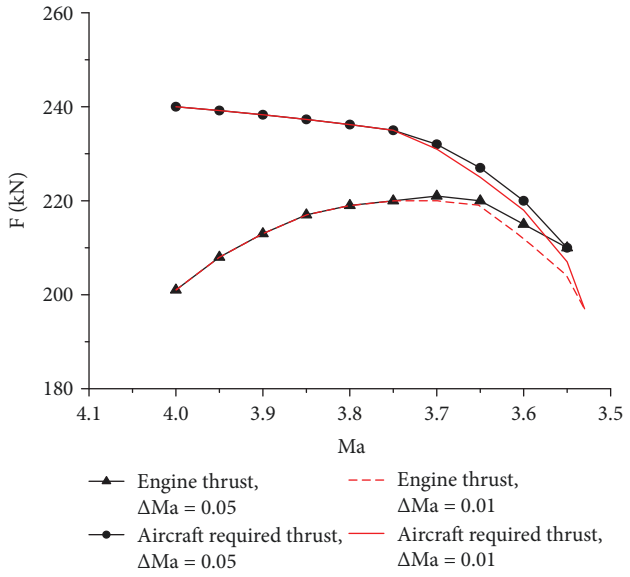

Figure 11: Influence of deceleration interval on Ma-F relation.

engines occurs single engine inoperative, the engines' total thrust cannot satisfy the aircraft required thrust. The aircraft will decelerate and descend quickly. Then, the engine will become the turbofan mode, where the Mach number is less than 3. Moreover, the maximum thrust of single engine of the turbofan mode is far less than the aircraft demanding thrust, which means the aircraft will decelerate and descend quickly, unable to find an alternate airport safely. When the three-engine one occurs single engine inoperative, the aircraft will decelerate and descend at first. Nevertheless, the gap between the engine thrust and the aircraft demanding thrust narrows; then, it can fly at a constant speed to find an alternate airport safely around Ma 3.55. When the four-engine one occurs single engine inoperative, because of the little difference between the aircraft demanding thrust and engine thrust, the aircraft can fly at a constant speed to find an alternate airport safely around Ma 3.89.

Thus, after the above calculation and analysis, considering single engine inoperative, it can be observed that three or four TBCC engines are needed for the Mach 4 supersonic civil aircraft in order to find an alternative airport safely. Then, considering the balance of the engine layout on the aircraft, four TBCC engines is a better choice for the Mach 4 supersonic civil aircraft.

According to the main operation points and thrust requirements of the studied supersonic civil aircraft scheme [26], the reference cruise L/D (7.79) of the Mach 4 supersonic aircraft [10], and the average climbing rate (30.5 m/s) of the Mach 4 supersonic aircraft scheme from NASA [27], the thrust requirements of TBCC engines for the Mach 4 supersonic civil aircraft are listed in Table 3.

4. Engine Jet Noise Prediction Model

For the new generation of the supersonic civil aircraft, the engine noise is an essential factor that should be taken into consideration during the schematic design phase so as to meet the airworthiness requirements. When the Mach 4 supersonic civil aircraft takes off, the TBCC engine works at the turbofan operating mode with the small bypass ratio, which causes quite high exhaust velocity. If the exhaust velocity is not restricted, it may cause the engine jet noise to dissatisfy the airworthiness requirements. Therefore, the engine jet noise prediction model is required to develop to assess the noise level of the concept. The index for evaluating the engine jet noise is the effective perceived noise level (EPNL), which can be calculated as shown in Figure 13 [28]. Firstly, based on the estimation of the engine jet noise prediction spectrum diagram, the perceived noise level (PNL) and perceived noise level with the tone correction (PNLT) as well as the effective perceived noise level (EPNL) can be calculated successively. Before the estimation of EPNL, the noise requirements of the Mach 4 supersonic civil aircraft should be determined. Based on Section 2, for the Mach 4 supersonic civil aircraft, it needs 4 TBCC engines and the W_{TO} is 407 tons (897,281 pounds). In view of this, EPNL should be less than 103 EPNdB to satisfy the noise requirements of FAR Part 36 [29].

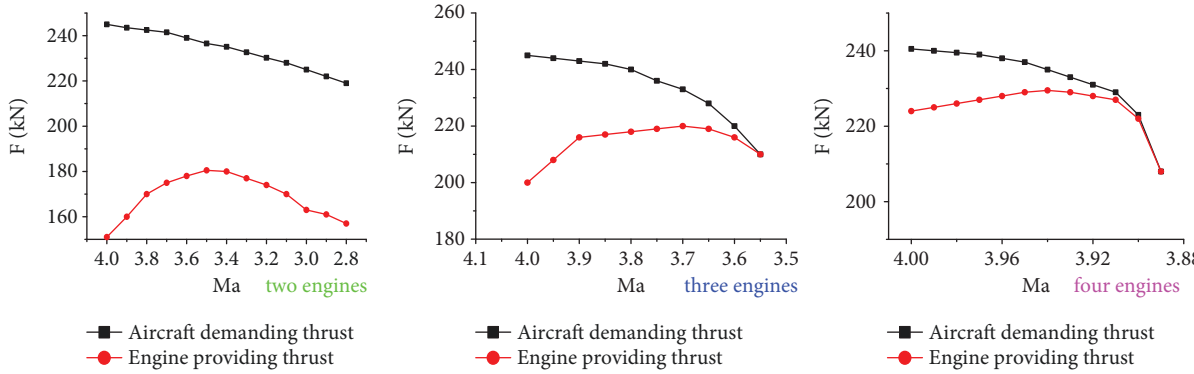

Figure 12: Curve of Ma-F (double, three, and four engines).

Table 3: Thrust requirements of the TBCC engine at main operation points.

	H (km)	Ma	Operation mode	Thrust (kN)
Take-off	0	0	Turbofan	4×240.2
Climb	20.9	3	Turbofan (design point)	4×150.6
Climb	25.0	4	Ramjet (design point)	4×137.2
Cruise	25.0	4	Ramjet	4×114.2

4.1. Engine Jet Noise Spectrum Prediction Model. This model provides the estimation of the engine jet noise spectrum for the Mach 4 supersonic civil aircraft. The commonly used prediction models include Stone model, Pao model, SAE model, and improved ICAO model [30]. In order to simplify the calculation and ensure the fidelity of the prediction model, these models should be compared with each other in order to choose the most suitable one. After comparison, only the Stone model input parameters can be achieved directly by the existing engine performance program and the measuring point layout of airworthiness requirements. In addition, the establishment of the Stone model is simpler when compared with other models, and its accuracy is also worth of trust. So, this section will use the Stone model to predict the Mach 4 TBCC engine jet noise spectrum. The flow chart of the engine jet noise spectrum prediction can be shown as Figure 14. The assumption of the Stone model is that the shock wave noise spectrum graphs of inner and bypass jet are independent, which could be calculated by the jet noise prediction method, respectively. Then, the integrated noise spectrum could be achieved by the superposition of the jet mixed noise, inner nozzle shock wave noise, and bypass nozzle shock wave noise [31, 32].

4.1.1. Subsonic Jet Noise Spectrum Prediction Model. This model is the spectrum prediction of subsonic jet noise of the Mach 4 TBCC engine. From Figure 14, it can be seen that the subsonic jet mixed noise can be divided into the inner jet noise and the bypass jet noise. Firstly, we should investigate the subsonic inner mixed jet noise spectrum which means the relation of the sound pressure level (SPL), the frequency parameter $\log S_1$, and the pole direction angle θ [33, 34]. And some of these parameters could be found in Table 4, which shows the relative position symbol of measuring point and nozzle.

According to the input parameters from the existing engine performance program and the measuring point layout of airworthiness requirements, in order to calculate SPL, the uncorrected overall sound pressure level (UOL_1) should be calculated in advance using the following equation [33, 34].

$$\begin{aligned}\mathrm{UOL}_1 = {} & 141 + 10\log\left[\left(\frac{\rho_a}{\rho_{ISA}}\right)^2 \cdot \left(\frac{c_a}{c_{ISA}}\right)^4\right] \\ & + 10\log\left(\frac{A_1}{R^2}\right) + 10\log\left(\frac{\rho_1}{\rho_a}\right)^{\omega} \\ & + 10\log\left(\frac{V_e}{c_a}\right)^{7.5} \\ & - 15\log\left[((1+M_c)\cdot\cos\theta)^2 + 0.04\cdot M_c^2\right] \\ & - 10\log\left[(1-M_0)\cdot\cos\varphi\right] \\ & + 3\log\left(\frac{2A_1}{\pi\cdot D_1^2} + \frac{1}{2}\right),\end{aligned} \tag{11}$$

where symbol ρ_a and c_a means the density (kg/m^3) and the speed of sound (m/s) under atmospheric environment, ρ_{ISA} and c_{ISA} means the density (kg/m^3) and the speed of sound (m/s) under standard atmospheric conditions, A_1 means the exit area of the inner nozzle (m^2), ρ_1 means the density (kg/m^3) of the inner jet, M_0 means the flight Mach number, and D_1 means the nozzle exit diameter (m). These cycle parameters and dimension parameters could be calculated by the existing TBCC engine model [22]. And coefficient ω is defined in (12). V_e means the effective velocity of inner jet, which can be calculated in (13). M_c means the convective Mach number, which is defined in (14).

$$\omega = \frac{3(V_e/c_a)^{3.5}}{0.6 + (V_e/c_a)^{3.5}} - 1, \tag{12}$$

$$V_e = V_1\left[1 - \left(\frac{V_0}{V_1}\right)\cos\alpha\right]^{2/3}, \tag{13}$$

$$M_c = \frac{0.62(V_1 - V_0\cos\alpha)}{c_a}, \tag{14}$$

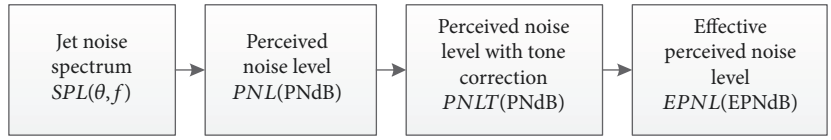

Figure 13: A simple procedure for estimating effective perceived noise levels from the spectrum.

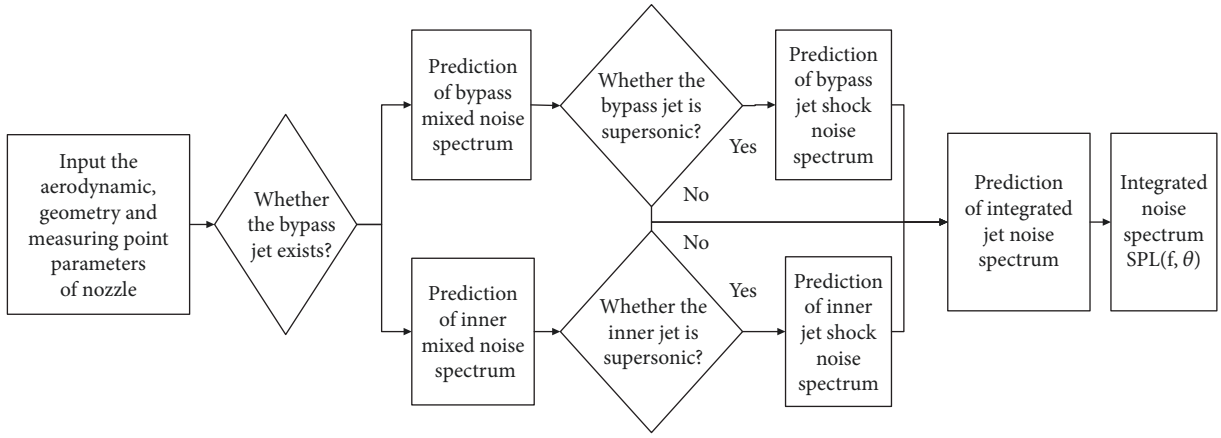

Figure 14: Prediction flow chart of the jet noise spectrum.

where V_0 and V_1 means the speed of the aircraft and inner jet and α means the angle between engine axis and flight direction. When engine axis and measuring points are on the same horizontal vertical plane, it means that $\alpha = \theta - \Psi$.

After the calculation of the uncorrected overall sound pressure level, in order to get the frequency parameter log S_1, the Strouhal number S_1 should be calculated in advance as follows.

$$S_1 = \frac{f\sqrt{4A_1/\pi}}{V_e}\left(\frac{D_1}{\sqrt{4A_1/\pi}}\right)^{0.4}[1 - M_0\cos\varphi] \times \frac{\left\{[1 + 0.62((V_1 - V_0)/c_a)\cos\theta]^2 + 0.01538((V_1 - V_0)/c_a)^2\right\}^{1/2}}{\left\{[1 + 0.62((V_1 - V)/c_a)\cos\theta]^2 + 0.01538(V_1/c_a)^2\right\}^{1/2}}. \quad (15)$$

Finally, according to the relation of SPL, the frequency parameter log S and the pole direction angle θ [33, 34], by interpolation, the relation of SPL, frequency f, and angle θ, could be got, which means the subsonic inner jet noise spectrum could be achieved.

According to Figure 14, it can be seen that the subsonic jet noise spectrum includes the inner jet noise spectrum and the bypass jet noise spectrum. After the estimation of the inner jet noise spectrum, the bypass jet noise spectrum should be calculated, which means that the area ratio, the temperature ratio, and the velocity ratio of inner and bypass should be considered to correct the corresponding parameters [35, 36]. By using the same method, the double jet mixed noise spectrum is achieved. It is also found that the influence of the bypass jet on spectrum is mainly reflected on the deviation of peak frequency of the sound pressure level. However, there is no monotonous relationship between the velocity ratio and the frequency deviation parameters [31, 32]. The bypass jet only affects slightly the inner jet mixed noise spectrum since the given area ratios are limited. In addition, as far as tandem-type TBCC engine applied in this article [22] is considered, the engine jet noise spectrum prediction model merely considers the influence of inner single jet without the bypass jet.

In order to evaluate the fidelity of the subsonic jet noise spectrum prediction model, the typical model-scale experimental data are selected as the reference in Table 5 [37], whose engine configuration is the dual-stream exhaust system with the subsonic jet. Meanwhile, the prediction results of the subsonic jet noise spectrum are compared with subsonic jet noise experimental data shown in Figure 15, where T_1, T_2, V_1, V_2, A_1, and A_2 mean the temperature, speed, and area of inner and bypass nozzle exit, which are determined by the experimental condition of jet noise [37]. From Figure 15, it can be seen that the prediction results agree well with the published experimental data. So, it proves that the fidelity of

Table 4: Relative position symbol of measuring point and nozzle.

Variable	Significance
R	Length between nozzle and measuring point
θ, theta	Pole direction angle (angle between engine axis and line connecting measuring point and nozzle)
ψ, psi	Modified pole direction angle (θ)
α, alpha	Engine angle of attack (angle between engine axis and flight direction)

Table 5: Subsonic jet noise spectrum experimental data [37].

Frequency (Hz)	SPL (dB)
101.5967	84.13
196.1021	90.27
483.4218	96.93
957.1784	101.47
1898.007	103.60
6007.91	102.00
9579.603	100.13

this noise spectrum estimation model is able to meet the requirements of the prediction of the engine jet noise.

Calculation condition is as follows: θ, theta = 90°, T_1 = 1129 K, V_1 = 593 m/s, T_2 = 280 K, V_2 = 216 m/s, and A_2/A_1 = 3.2.

$$A_1 = \frac{1}{4}\pi D_1^2 = \frac{1}{4} \times \pi \times 0.1^2 = 0.00785\ \mathrm{m}^2. \tag{16}$$

4.1.2. Supersonic Jet Noise Spectrum Prediction Model. This model provides the prediction method of calculating the supersonic jet noise spectrum. From Figure 14, it can be seen that when compared with the subsonic jet, the supersonic jet noise could be divided into the jet mixed noise and the shock wave noise. In order to estimate the shock wave noise spectrum, which is similar to the subsonic jet mixed noise, the sound pressure level SPL, the frequency parameter $\log S_1$, and the pole direction angle θ should be calculated in advance.

Firstly, the uncorrected overall sound pressure level of shock wave noise ($\mathrm{UOL}_{s,j}$) can be calculated as follows [33, 34].

$$\begin{aligned}\mathrm{UOL}_{s,j} = {} & 162 + 10\log\left[\left(\frac{\rho_a}{\rho_{ISA}}\right)^2 \cdot \left(\frac{c_a}{c_{ISA}}\right)^4\right] \\ & + 10\left(\frac{A_j}{R^2}\right) + 10\log\left[\frac{\left(M_j^2 - 1\right)^2}{1 + \left(M_j^2 - 1\right)^2}\right] \\ & - 10\log\left[(1 - M_0) \cdot \cos\varphi\right] + F \cdot (\theta - \theta_M),\end{aligned} \tag{17}$$

where A_j means the exit area of nozzle (m^2) and M_j means the jet Mach number, which could be calculated by the existing TBCC engine performance model [22]. And parameters θ_M and F are defined in (18) and (19), respectively.

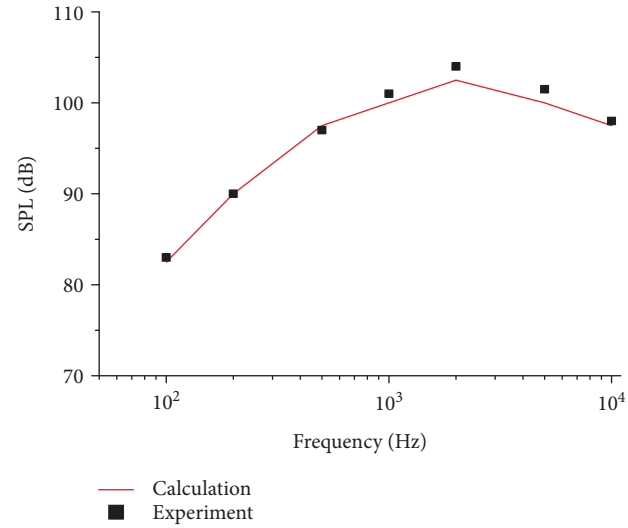

Figure 15: The check of the subsonic jet noise spectrum.

$$\theta_M = 180\ \mathrm{deg} - \sin^{-1}\left(\frac{1}{M_j}\right), \tag{18}$$

$$F = \begin{cases} = 0 & (\theta \le \theta_M), \\ = -0.75 & (\theta > \theta_M). \end{cases} \tag{19}$$

Then, the Strouhal number $S_{s,j}$ can be calculated as follows:

$$\begin{aligned} S_{s,j} = {} & \left(\frac{fD_j}{0.7V_j}\right)\sqrt{M_j^2 - 1}(1 - M_0\cos\varphi) \\ & \times \sqrt{\left[1 + 0.7\left(\frac{V_j}{c_a}\right)\right]^2 + 0.0196\left(\frac{V_j}{c_a}\right)}, \end{aligned} \tag{20}$$

where D_j and V_j mean the exit diameter of the nozzle and the speed of the jet, which could be calculated by the TBCC engine performance model [17]. Based on the similarity with the calculation of subsonic jet noise spectrum, the shock wave noise spectrum could be achieved.

Next, referring to the computing method of the subsonic jet mixed noise spectrum, the spectrum of supersonic jet noise could be got. Finally, the supersonic comprehensive jet noise spectrum can be achieved by a superposition of the jet mixed noise, inner nozzle shock wave noise, and bypass nozzle shock wave noise [31, 36].

Being similar to the verification of the subsonic jet noise spectrum, in order to evaluate the accuracy and availability of the supersonic jet noise spectrum prediction model, the typical model-scale experimental data are selected as the reference in Table 6 [37], whose engine configuration is a dual-stream exhaust system with the supersonic jet. What is

Table 6: Supersonic jet noise spectrum experimental data [37].

Frequency (Hz)	SPL (dB)
125.4961	96.63934
197.6471	98.48361
398.1072	101.5574
1287.031	108.1148
2592.38	112.8279
4082.808	118.1557
5123.763	118.9754
6552.973	115.6967
8223.723	115.082
10,320.45	113.8525

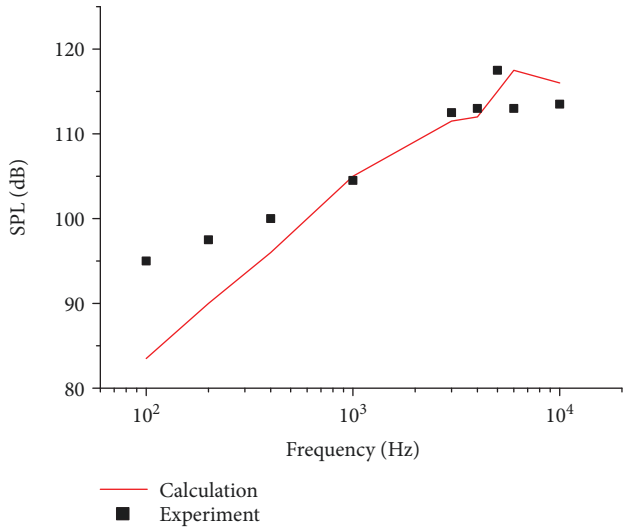

Figure 16: The check of the supersonic jet noise spectrum.

more, the prediction results of the supersonic jet noise spectrum are compared with the published experimental data shown in Figure 16, where M_1 means the Mach number of inner jet and the calculation condition is determined by the experimental condition of jet noise [37]. From Figure 16, it can be observed that the prediction results also match well with the experimental results. So, it proves that the accuracy of this noise spectrum estimation model is able to meet the requirements of the prediction of the engine jet noise.

Calculation condition is as follows: θ, theta = 95°, T_1 = 1127 K, V_1 = 790 m/s, M_1 = 1.38, T_2 = 283 K, V_2 = 218 m/s, and A_2/A_1 = 1.9

$$A_1 = \frac{1}{4}\pi D_1^2 = \frac{1}{4} \times \pi \times 0.101^2 = 0.00801\ \text{m}^2. \tag{21}$$

4.2. The Prediction Method of an Effective Sensory Noise Level. From Figure 10, it can be seen that after the jet noise spectrum prediction model is built, PNL, PNLT, and EPNL could be calculated successively to evaluate the engine jet noise [28].

4.2.1. Perceived Noise Level (PNL). Based on the jet noise spectrum, to estimate PNL, the function of frequency and sound pressure level N_{i}, as well as accumulative total noise N_{t} should be introduced, which can be defined in (22) and (23), respectively.

$$N = \begin{cases} 0 \quad (\text{SPL} < A1), \\ 10^{B1(\text{SPL}-A1)^{-1}} \quad (A1 \le \text{SPL} < A2), \\ 10^{B2(\text{SPL}-A2)} \quad (A2 \le \text{SPL} < A3), \\ 10^{B3(\text{SPL}-A3)} \quad (A3 \le \text{SPL} < A4), \\ 10^{B4(\text{SPL}-A4)} \quad (A4 \le \text{SPL} < 150), \end{cases} \tag{22}$$

$$\begin{aligned} N_{\text{t}} &= N_{\max} + 0.15\left[\left(\sum_{i=1}^{24} N_i\right) - N_{\max}\right] \\ &= 0.85N_{\max} + 0.15\left(\sum_{i=1}^{24} N_i\right), \end{aligned} \tag{23}$$

where $A1$, $B1$, etc. are all coefficients, which are determined by the central frequency of 1/3 frequency range. PNL means the single numerical expression of the noise annoyance level, which can be calculated as follows.

$$\text{PNL} = 40.0 + \frac{10}{\log 2} \log N_{\text{t}} = 40.0 + 33.22 \log N_{\text{t}}. \tag{24}$$

4.2.2. Perceived Noise Level with Tone Correction (PNLT). Because human auditory system has the predilection for following a single tone rather than the wide-band noise in the adjacent frequency range, the perceived characteristic of the single tone should be considered. The purpose of single tone correction is to detect the pure tone which includes 1/3 frequency range and to correct its influence at the same time. To achieve PNLT, the specific steps are shown as follows:

(1) The second-order elementary errors should be calculated

(2) If SPL_i is local maximum, the average noise level or background noise level and their differences should be calculated

(3) The discrete frequency correction C should be determined, and its maximum $C_{\max}$ should be found

(4) PNLT could be calculated as follows

$$\text{PNLT} = \text{PNL} + C_{\max}. \tag{25}$$

4.2.3. Effective Perceived Noise Level (EPNL). The basic evaluation criterion for aircraft noise qualification is EPNL, which involves the sound level, the frequency distribution, and the time variation of noise. More concretely, it needs to record the instant SPL per 0.5-second interval. Meanwhile, the period of time around the maximum value of PNLT has the greatest impact on EPNL. However, due to the lack of

specific take-off track, in this section, the calculation of EPNL needs to be simplified. It is assumed that in the range of time recording, the maximum PNLT almost has no difference with all other PNLT and they are equivalent, which means EPNL equals to PNLT.

Thus, the jet noise prediction model is achieved, which can estimate EPNL fast and simply. And its input parameters can be provided by the TBCC engine performance model [22]. So, a quick and trusted model is established in this section to predict the Mach 4 supersonic civil aircraft engine jet noise level.

5. NO_x Emission Prediction Model

Similar to the engine noise, the Mach 4 supersonic civil aircraft engine NO_x emission is also an essential factor that should be considered in the schematic design phase. It is because the airworthiness regulations have strict restrictions on the engine NO_x emission which could cause great damages to the ozone layer and lead to the serious environmental pollution. The index for evaluating the engine pollutant emission (EI) could be defined in (26) [38]. According to the NASA research program of the new generation of the supersonic aircraft, the target value of the NO_x emission index should be less than 10 g/kg fuel consumption during cruise [39]. Thus, to meet the airworthiness regulations, after the comparison and the analysis of the NO_x emission prediction method, the most appropriate way to estimate the Mach 4 supersonic civil aircraft engine NO_x emission is shown as follows.

$$\mathrm{EI} = \frac{\text{pollutant emission (g)}}{\text{fuel consumption (kg)}}. \tag{26}$$

5.1. Comparison of Different NO_x Emission Prediction Methods. At present, there are about three kinds of modeling methods for the NO_x emission prediction: modified model method, reactor model method, and CFD numerical simulation method [40–42]. Compared with other methods, the input parameters of the modified model method could be achieved from the existing engine performance program directly and its modeling process is more concise. Based on the aforementioned analysis, the modified model method is chosen to estimate $\mathrm{EINO_x}$ in this article. At the same time, the three emission prediction models of the modified model method will be analyzed and compared so as to choose the most accurate and suitable one to calculate $\mathrm{EINO_x}$ of the supersonic civil aircraft engine.

5.1.1. T_3 Model Method. T_3 model method is based on the NO_x emission and the combustion chamber entrance total temperature T_{t3}, according to the study by Tsague et al. [38], which has a high fitting precision, and its relation could be shown as follows.

$$\mathrm{EINO_x} = 4 \times 10^{-9} T_{t3}^{3.364}. \tag{27}$$

5.1.2. HSCT Method. HSCT method is based on the NASA research about the supersonic civil aircraft [43], whose prediction algorithm could be shown in (28), where subscript "toc" denotes the top-of-climb cycle conditions, $T_{t3\ \max}$ means the highest compressor discharge total temperature, P_{t4} and T_{t4} mean the combustor exit total pressure and temperature, Wa means the combustor airflow, and T_f means the combustor flame total temperature.

When $T_3 < 611$ K,

$$\mathrm{EINO_x} = 0.01555 T_{t3} - 8.3. \tag{28}$$

When $T_3 \geq 611$ K,

$$\mathrm{EINO_x} = 2.899 \left(\frac{T_{t3\ \max}}{1000} - 0.46 \right) \left(\frac{P_{t4}}{P_{t4toc}} \frac{T_{t4toc}}{T_{t4}} \frac{W a_{toc}}{W_a} \right) \times \exp\left(-72.28 + 2.078 \sqrt{T_f} - 0.014611 T_f \right). \tag{29}$$

5.1.3. DLR Fuel Method. The specific steps of the DLR fuel method can be shown as follows [44]. At first, the equivalent fuel mass flow $W_{f,cor}$ of ground state should be calculated as shown in (30), where W_f means the fuel mass flow of the ground state, δ_t means the ratio of inlet entrance total pressure and atmospheric pressure, and θ_t means the ratio of inlet total temperature and standard atmospheric temperature. Then, $\mathrm{EINO_x}$ of the reference state could be achieved by interpolation, due to its unique functional relationship with equivalent mass flow for the same engine. Finally, $\mathrm{EINO_x}$ of the operating point could be calculated as shown in (31).

$$W_{f,cor} = \frac{W_f}{\delta_t \sqrt{\theta_t}}, \tag{30}$$

$$\mathrm{EINO_x} = \delta_t^a \theta_t^b \mathrm{EINO_{x,ref}}, \tag{31}$$

where a and b are the empirical fitting parameters, the range of a is 0.4–0.5, and b equals 3; meanwhile, the relation of $\mathrm{EINO_x}$ and combustion chamber inlet temperature T_3 and pressure P_3 of the reference state could be shown as follows.

$$\mathrm{EINO_{x,ref}} = \mathrm{const} P_{3,cor}^a T_{3,cor}^b, \tag{32}$$

where the combustion chamber inlet temperature T_3 and pressure P_3 of the reference state can be calculated in (33) and (34), respectively.

$$P_{3,cor} = \frac{P_3}{\delta_t}, \tag{33}$$

$$T_{3,cor} = \frac{T_3}{\theta_t}. \tag{34}$$

After the introduction of these $\mathrm{EINO_x}$ prediction methods, several engines are used as cases to evaluate their accuracy and availability. Firstly, using the PW4056 engine [44] as an example to check the accuracy of the HSCT method, Figure 17 shows the effect of different T_f on emission prediction estimated by the HSCT method.

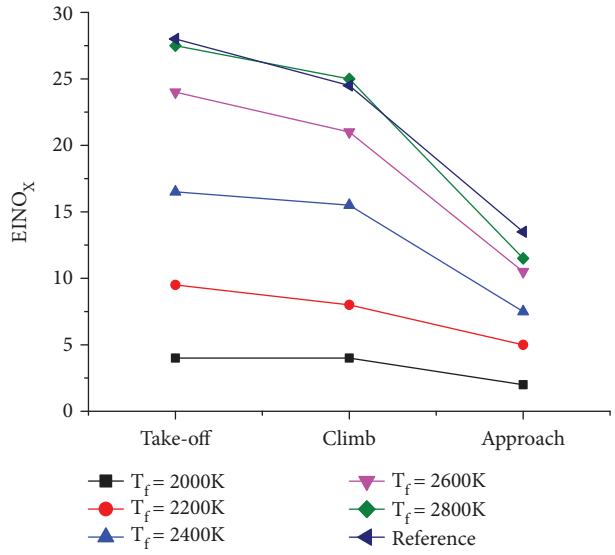

Figure 17: Effect of different T_f on emission prediction.

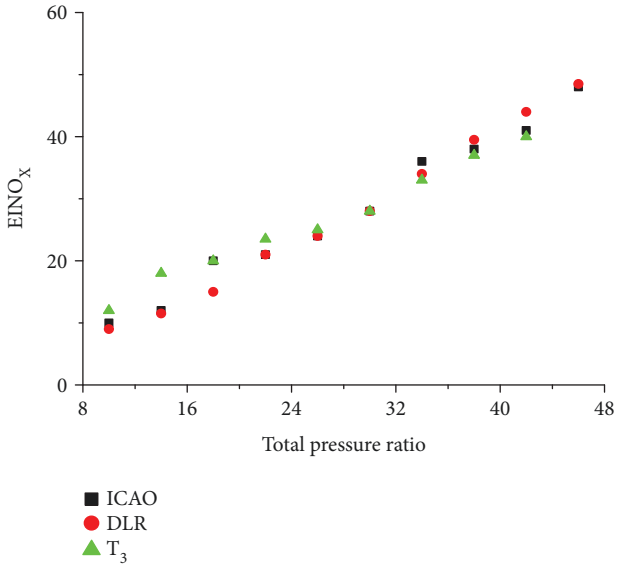

Figure 18: Prediction precision comparison between the methods with ICAO database.

According to Figure 17, it can be seen that the flame temperature has significant influence on EINO$_x$ when using the HSCT method. However, the flame temperature is difficult to estimate precisely in the TBCC engine performance model [22], so the HSCT method may not meet the requirements of accuracy.

Then, ICAO database [45] is used to check the precision of T_3 model and DLR fuel methods. The prediction precision comparison of the two methods is shown in Figure 18.

According to Figure 18, it is shown that the fitting curve of the DLR fuel method is more precise than the T_3 method referring to ICAO data. Therefore, the DLR method is used to predict the EINO$_x$ of the Mach 4 supersonic civil aircraft engine.

6. Multiobjective Optimization Module

After considering the aforementioned investigation of task requirement analysis, jet noise, and NO$_x$ emission prediction model of the Mach 4 supersonic civil aircraft TBCC engine, this module provides the optimization of the engine design parameters and control law, in order to get better engine performance, lower noise, and lower emissions. Due to the large quantities of engine variables (twelve variables) to be optimized, sensitivity analysis should be used first to conduct the preliminary screening and reduce the number of optimal variables. The polynomial combination of the response surface method is then used to simplify the target value calculation in the optimization process, based on the precise but time-consuming nonlinear component-based engine performance program. Considering the great number of optimization objectives (seven optimization objectives), the most mature, widely used multiobjective genetic algorithm is used to optimize the above performance index. Because the operating modes of the TBCC engine are divided into turbofan mode, ramjet mode, and mode conversion point, the optimization schemes should be divided into the above three modes as shown in Figure 19. And the specific optimization progress is presented as below.

6.1. Optimization of the Ramjet Mode. This section provides the optimization of the ramjet mode. Before the specific optimal calculation, the optimization objectives and constraints should be determined at first. The objective is to decrease SFC at ramjet design point and to reduce SFC and emissions at cruising point. Then, according to Table 3, the constraints are summarized as follows.

(i) Engine thrust to be kept more than 137.2 kN (design point)

(ii) Engine thrust to be kept more than 114.2 kN (cruising point)

According to the above content, it can be seen that there are several performance indicators needed to be analyzed and optimized. The sensitivity analysis should be made to preselect the design parameters and control law, in order to reduce the number of optimization goals and simplify the difficulty of optimization. The performance sensitivity analyses at ramjet mode design point are shown in Figures 20 and 21 which also indicate the relative changes in performance influenced by the 5% increase of the independent variables. Moreover, the TBCC engine performance model is used to carry out the complete calculation [22].

As shown in Figure 20, for design point performance, decreasing the afterburner exit total temperature T_{t7} makes the fuel consumption and emissions decrease. At the same time, increasing the inlet flow Wa makes thrust meet the demand.

As shown in Figure 21, for cruising performance, decreasing the control law of T_{t7} ($T_{t7control}$) and control law of the nozzle throat area A_8 ($A_{8control}$) at off-design point makes the cruising fuel consumption decrease. At the same time, increasing the inlet flow Wa and T_{t7} at design point

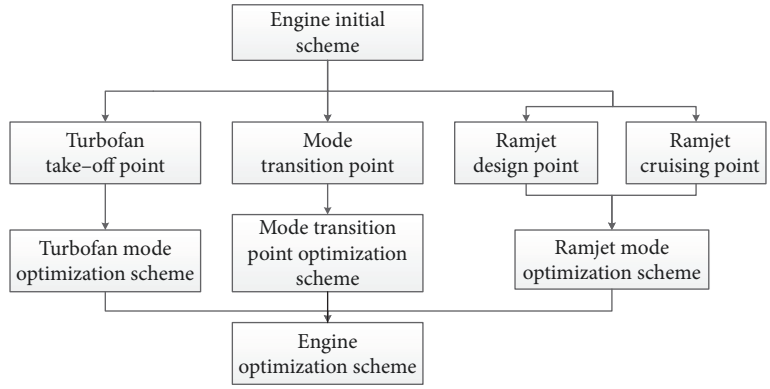

Figure 19: Optimization scheme of the TBCC engine.

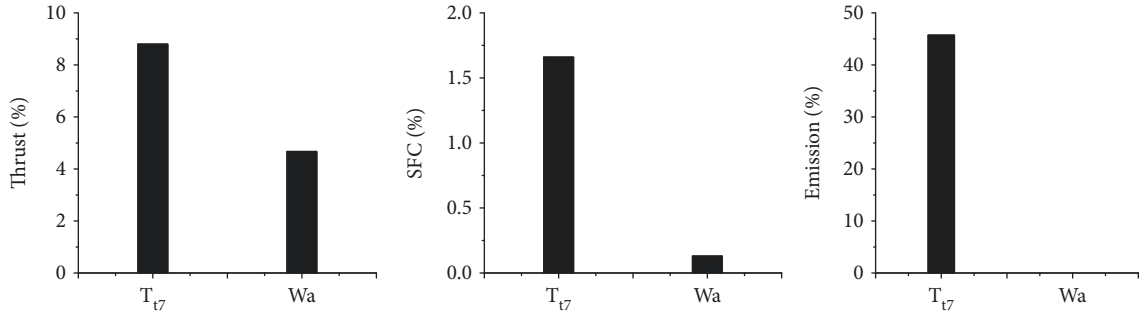

Figure 20: Sensitivity analysis of the ramjet mode at design point.

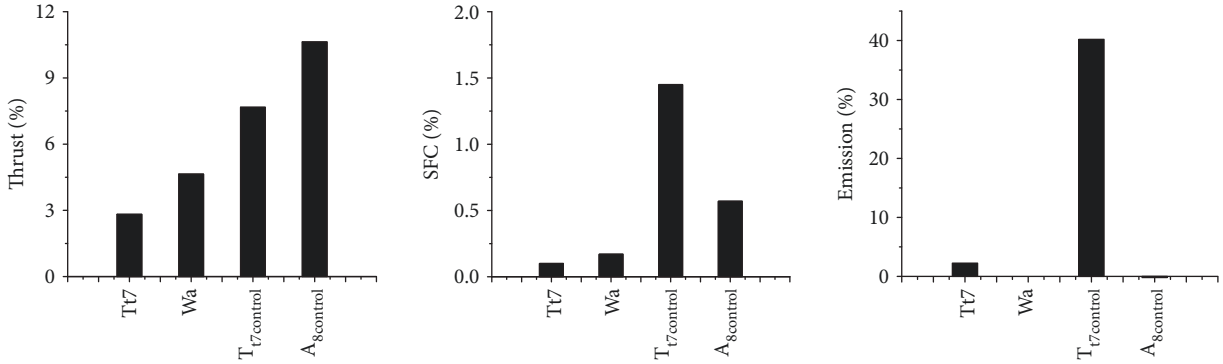

Figure 21: Sensitivity analysis of the ramjet mode at cruising point.

makes the cruising thrust meet the constraints. However, it is found that T_{t7} at cruising point corresponding to the minimum of cruising emissions changes with T_{t7} at design point. Thus, the sensitivity analysis could not confirm the specific values of these parameters, and the automatic optimization of genetic algorithm should be used to find the optimum solution shown as below. To express more conveniently and improve the versatility of the optimization method, the range $[x_1, x_2]$ of independent variables is transformed into the coding interval $[-1, 1]$ shown in (35), where x and x_{code} mean the previous value and the code value of the parameter, while $[x_1, x_2]$ means the adjustable interval of the parameter. The response surface method is also used for polynomial fitting to replace the difficult engine performance simulation, where the design point parameters and the control laws are the input variables. Finally, the multiobjective genetic algorithm is used to optimize the engine parameters of design point and cruising operating point as shown in Table 7. What is more, it can be seen that SFC and $EINO_x$ have significant decrease, the reduction of outlet temperature of combustion chamber could simplify its design, and increasing A_8 and air mass flow makes it meet the thrust demand. According to the above content, the optimization of the ramjet mode achieves the optimization goals.

$$x_{code} = \frac{x - x_1}{x_2 - x_1} - 1. \tag{35}$$

6.2. Optimization of the Mode Transition Point. According to Figure 19, after the optimization of the ramjet mode, this

Table 7: Ramjet mode optimization scheme (design and cruising point).

Ramjet design point	Before optimization	After optimization	Cruising operating point	Before optimization	After optimization
Flight altitude (km)	25	25	Flight altitude (km)	25	25
Flight Mach	4	4	Flight Mach	4	4
Thrust (kN)	138.3	138.4	Thrust (kN)	115.0	114.9
SFC (kg/daN/h)	2.00	1.97	SFC (kg/daN/h)	1.98	1.908
Air mass flow (kg/s)	208	227	Air mass flow (kg/s)	228	267
Outlet temperature of the combustion chamber (T_{t7}) (K)	2000	1909	Outlet temperature of the combustion chamber (T_{t7}) (K)	1730	1614
Maximum area of A_8 (m^2)	2.3	2.4	A_8 (m^2)	0.95	1.06
$EINO_x$ (g/kg)	10.87	7.11	$EINO_x$ (g/kg)	4.97	4.74

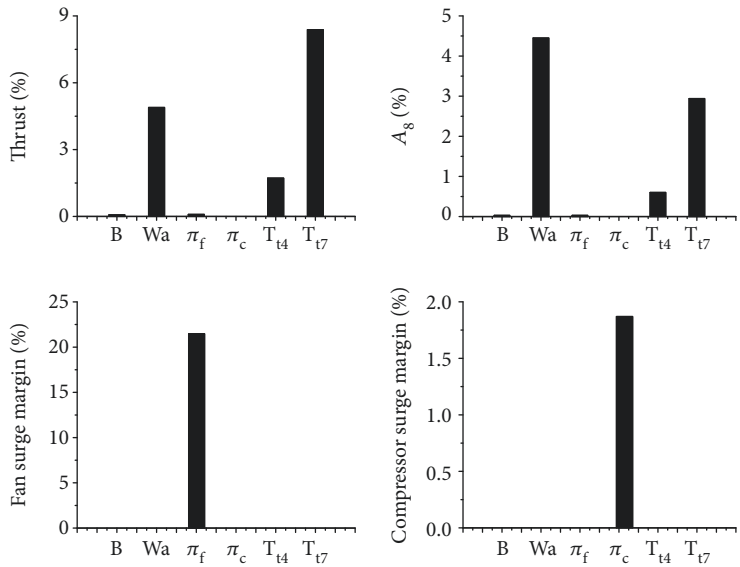

Figure 22: Sensitivity analysis of the mode transition point (design point of the turbofan mode).

section provides the optimization of the mode transition point, which is also the design point of the turbofan mode. The optimization objectives are to minimize A_8 of the ramjet mode at mode transition point to simplify its design difficulty. The constraints are summarized as follows, where the constraint of engine thrust at mode transition point refers to Table 3.

(i) Enough surge margin for the fans and the compressors

(ii) Total flow rate to be kept almost constant during the mode transition

(iii) Engine thrust to be kept almost constant and more than 151.6 kN

Performance sensitivity analysis at the ramjet mode design point are shown in Figure 22 which also indicates the relative changes in performance influenced by the 5% increase of the independent variables, where B means the bypass ratio and π_f and π_c mean the pressure ratio of fan and compressor, respectively. Except for A_8, all the parameters belong to the turbofan mode. Similar to the ramjet mode, the sensitivity analysis of the mode transition point is made on the basis of the TBCC engine performance model [22]. Figure 22 shows that for mode transition point performance, increasing Wa, T_{t4}, and T_{t7} makes the thrust and A_8 increase. However, bypass ratio and pressure ratio have little influence on them and the compressor and fan surge margin is only influenced by their own pressure ratio at design point. Because the fan margin is adequate, the fan pressure ratio is set to be 1.3 without optimization referring to the TBCC engine performance model [22]. Increasing T_{t4} leads to the increase of design point thrust but slightly increases of A_8. Therefore, according to the above analysis, T_{t4} is tentatively determined as a higher value of 2000 K [22]. Other optimization variables are difficult to value, so the response surface method and multiobjective genetic algorithm are used to calculate the performance parameters and optimize the above performance index. The turbofan mode optimization scheme is shown in Table 8, where increasing afterburner temperature and bypass ratio results in the increase of thrust. Then, according to the relationship between the thrust, air mass flow, and control law at mode

Table 8: Turbofan mode optimization scheme.

Design point (mode transition point)	Before optimization	After optimization
Flight altitude (km)	20.9	20.9
Flight Mach	3	3
Thrust (kN)	151.8	157
SFC (kg/daN/h)	1.61	1.62
Air mass flow (kg/s)	318	318.5
Bypass ratio	0.7	0.74
Outlet temperature of the main combustion chamber (K)	2000	2000
Afterburner temperature (K)	1350	1377

Table 9: Ramjet mode optimization scheme at mode transition point.

	Before optimization	After optimization
Flight altitude (km)	20.9	20.9
Flight Mach	3	3
Thrust (kN)	151	157
SFC (kg/daN/h)	1.8	1.8
Air mass flow (kg/s)	318	318
T_{t7} (K)	1400 K	1425 K
Maximum area of A_8 (m^2)	2.3	2.4

transition point, the ramjet mode optimization scheme at mode transition point is shown as Table 9. According to the optimization constraint of the constant engine thrust at mode transition point, the T_{t7} of the ramjet mode should be increased. To keep the mass flow constant through the outlet nozzle, the A_8 should be increased, which can meet the optimization objective at mode transition point.

6.3. Optimization of the Turbofan Mode. According to Figure 19, after the above optimization, the turbofan mode is optimized successively. Before the specific optimal calculation, the optimization objectives and constraints should be determined at first. The objective is to get the reduction of the noise level and emission at take-off point. Then, the constraints are summarized as follows.

(i) Constraints of engine thrust

(ii) Constraints of margin of the fan and compressor

The polynomial combination of the response surface method is used to calculate the target value. The multiobjective genetic algorithm is used to optimize the engine performance index. The optimization scheme is shown in Table 10. It can be observed that, increasing bypass ratio makes the exhaust velocity, SFC, and $EINO_x$ decrease. At the same time, the drawbacks of the increasing BPR is the reduction of inner flow capacity and specific thrust. But the increase of the outlet temperature of the main combustion chamber and the air mass flow makes the thrust satisfy its

Table 10: Turbofan mode optimization scheme.

Take-off operating point	Before optimization	After optimization
Flight altitude (km)	0	0
Flight Mach	0	0
Thrust (kN)	241.8	240.3
SFC (kg/daN/h)	0.82	0.817
Bypass ratio	1.24	1.4
Air mass flow (kg/s)	556	570
Outlet temperature of the main combustion chamber (K)	1545	1557
Exhaust velocity (m/s)	425.6	412
Noise level (EPNdB)	102.95	102.43
$EINO_x$ (g/kg)	6.37	5.47

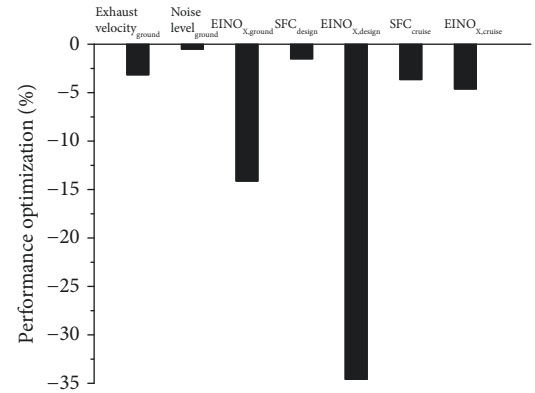

Figure 23: Optimization results of TBCC engine performance.

constraint. The reduction of $EINO_x$ and noise level makes the realization of the optimization objectives.

Thus, on the basis of the tandem TBCC engine performance model [22], the optimization of the TBCC engine is completed and its results could be seen in Figure 23. It can be seen that the $EINO_x$, SFC, and exhaust velocity of the nozzle have been greatly reduced and the noise level also has a certain reduction. Thus, the developed multiobjective optimization tool is able to optimize the design parameters and the control law of the Mach 4 supersonic civil aircraft TBCC engine, in order to get its conceptual design with better performance, lower noise, and lower emissions. Finally, its task requirements could be satisfied.

7. Conclusion

The conceptual design and performance optimization of the propulsion system is extremely important for the Mach 4 supersonic civil aircraft. Integration of the most important calculation and analysis modules into one simulation platform provides the benefits which means the conceptual scheme, noise level, emission prediction, and performance optimization can be considered simultaneously and systematically. To meet the above objectives, a quick and trusted numerical simulation platform is established to analyze the

Mach 4 TBCC engine concept for the supersonic civil aircraft, which includes the newly developed task requirement analysis module, engine jet noise, and the NO_x emission prediction models, as well as a multiobjective optimization tool based on the response surface methodology. Therefore, some useful conclusions can be drawn.

(1) Using an aircraft preliminary weight estimation method and the sensitivity analysis of parameters, a preliminary concept supersonic civil aircraft can be achieved with details of cruising Mach 4, range 10,000 km, capacity of 300 people, and fuel efficiency figure of merit 14.8 PAX·km/kg

(2) The TBCC engine performance simulation model is used as the propulsion system of the Mach 4 supersonic civil aircraft. If one engine on the aircraft is inoperative during the cruising condition, considering the requirements of finding an alternative airport safely and the balance of the engine layout on the aircraft, four TBCC engines will be needed for the Mach 4 supersonic civil aircraft

(3) Utilizing the developed platform, under the requirements of noise, emission, and engine thrust, as well as aerodynamic and structural compatibility of two modes, the main design parameters of the Mach 4 TBCC engine are shown as follows: at take-off point, T_{t4} 1557 K and bypass ratio 1.4; at mode conversion point, T_{t4} 2000 K, bypass ratio 1.62, fan pressure ratio 1.3, and compressor pressure ratio 2.7; at ramjet design point, T_{t4} 1909 K; and at cruising operating point, T_{t4} 1614 K

(4) A multiobjective optimization tool can be used to optimize the conceptual design of Mach 4 TBCC engines with better performance, lower noise, and lower emissions, based on optimizing design parameters and control law of TBCC engines, which makes $EINO_{x,design}$ −35.49%, SFC_{design} −1.50%, $EINO_{x,cruise}$ −4.62%, SFC_{cruise} −3.64%, $\text{noise level}_{ground}$ −0.51%, and $\text{exhaust velocity}_{ground}$ −3.15%. Finally, the optimized conceptual design of the TBCC engine could meet its task requirements

Data Availability

The data used to support the findings of this study are included within the article.

Conflicts of Interest

The authors declare that they have no conflicts of interest.

Acknowledgments

This research is funded by the National Nature Science Foundation of China (NSFC) under Grants 51776010 and Project MIIT. The authors are thankful for the support from Collaborative Innovation Center of Advanced Aero-Engine.

References

[1] J. J. Berton, W. J. Haller, P. F. Senick, S. M. Jones, and J. A. Seidel, *A Comparative Propulsion System Analysis for the High-Speed Civil Transport*, NASA TM-2005, 2005.

[2] D. R. Reddy, "Seventy years of aeropropulsion research at NASA Glenn Research Center," *Journal of Aerospace Engineering*, vol. 26, no. 2, pp. 202–217, 2013.

[3] L. Foster, J. Saunders, B. Sanders, and L. Weir, "Highlights from a Mach 4 experimental demonstration of inlet mode transition for turbine-based combined cycle hypersonic propulsion," in *48th AIAA/ASME/SAE/ASEE Joint Propulsion Conference & Exhibit*, Atlanta, GA, USA, August 2012.

[4] C. S. Domack, S. M. Dollyhigh, F. L. Beissner Jr et al., *Concept Development of a Mach 4 High-Speed Civil Transport*, NASA-TM-4223, 1990.

[5] A. W. Robins, S. M. Dollyhigh, F. L. Beissner Jr et al., *Concept Development of a Mach 3.0 High-Speed Civil Transport*, NASA TM-4058, 1988.

[6] H. R. Welge, J. Bonet, T. Magee et al., *N+2 Supersonic Concept Development and Systems Integration*, NASA/CR-2010-216842, 2010.

[7] J. Morgenstern, M. Buonanno, J. Yao et al., *Advanced Concept Studies for Supersonic Commercial Transports Entering Service in the 2018-2020 Period Phase 2*, NASA/CR-2015-218719, 2015.

[8] H. Robert Welge, J. Bonet, T. Magee et al., *N+3 Advanced Concept Studies for Supersonic Commercial Transport Aircraft Entering Service in the 2030-2035 Period*, NASA/CR-2011-217084, 2011.

[9] J. Morgenstern, N. Norstrud, M. Stelmack, and C. Skoch, *Final Report for the Advanced Concept Studies for Supersonic Commercial Transports Entering Service in the 2030 to 2035 Period, N+3 Supersonic Program*, NASA/CR-2010-216796, 2010.

[10] J. Steelant, "Achievement obtained for sustained hypersonic flight within the LAPCAT project," in *15th AIAA International Space Planes and Hypersonic Systems and Technologies Conference*, pp. 2008–2578, Dayton, OH, USA, 2008.

[11] J. Steelant, "LAPCAT: high-speed propulsion technology," in *Advances on Propulsion Technology for High-Speed Aircraft*, pp. 12-1–12-38, Neuilly-sur-Seine, France, 2008.

[12] J. Steelant, "Sustained hypersonic flight in Europe: technology drivers for LAPCAT II," in *16th AIAA/DLR/DGLR International Space Planes and Hypersonic Systems and Technologies Conference*, Bremen, Germany, 2009.

[13] L. Serre and S. Defoort, "LAPCAT II: towards a Mach 8 civil aircraft concept, using advanced rocket/dual-mode ramjet propulsion system," in *16th AIAA/DLR/DGLR International Space Planes and Hypersonic Systems and Technologies Conference*, pp. 720–735, Bremen, Germany, 2009.

[14] K. Sakata, "Supersonic experimental airplane (NEXST) for next generation SST technology," in *40th AIAA Aerospace Sciences Meeting & Exhibit*, Reno, NV, USA, 2002.

[15] T. Ohnuki, K. Hirako, and K. Sakata, "National experimental supersonic transport project," in *International Congress of the Aeronautical Science*, Daejeon, South Korea, 2006.

[16] A. Murakami, *Silent Supersonic Technology Demonstration Program*, ICAS, 2006.

[17] P. Dong, H. Tang, M. Chen, and Z. Zou, "Overall performance design of paralleled heat release and compression system for

hypersonic aeroengine," *Applied Energy*, vol. 220, pp. 36–46, 2018.

[18] J. Zheng, H. Tang, M. Chen, and F. J. Yin, "Equilibrium running principle analysis on an adaptive cycle engine," *Applied Thermal Engineering*, vol. 132, pp. 393–409, 2018.

[19] J. Zheng, M. Chen, and H. Tang, "Matching mechanism analysis on an adaptive cycle engine," *Chinese Journal of Aeronautics*, vol. 30, no. 2, pp. 706–718, 2017.

[20] P. Dong, H. Tang, and M. Chen, "Study on multi-cycle coupling mechanism of hypersonic precooled combined cycle engine," *Applied Thermal Engineering*, vol. 131, pp. 497–506, 2018.

[21] M. Chen, J. Zhang, and H. Tang, "Performance analysis of a three-stream adaptive cycle engine during throttling," *International Journal of Aerospace Engineering*, vol. 2018, Article ID 9237907, 16 pages, 2018.

[22] M. Chen, H. Tang, K. Zhang, O. Hui, and Y. Wang, "Turbine--based combined cycle propulsion system integration concept design," *Proceedings of the Institution of Mechanical Engineers, Part G: Journal of Aerospace Engineering*, vol. 227, no. 7, pp. 1068–1089, 2012.

[23] W. Li, *Aircraft Overall Design*, Northwestern Polytechnical University, Xi'an, China, 2005.

[24] A. Ade, *Aerodynamic Design of Transport Aircraft*, S. Gu, X. Wu, and X. Y. Trans, Eds., Shanghai Jiao Tong University, Shanghai, China, 2010.

[25] K. Shimizu and N. Nogami, "Current status of low pressure turbine component research in HYPR program," in *34th AIAA/ASME/SAE/ASEE Joint Propulsion Conference and Exhibit*, Cleveland, OH, USA, 1998.

[26] M. Chen, *Research on the Tandem Scheme of Hypersonic Turbine/Ramjet Combined Engine [Ph.D. thesis]*, Beihang University, Beijing, China, 2007.

[27] G. Xiao, *Aeroengine Design Manual*, vol. 5, Aviation Industrial Publishing House, Beijing, China, 1998.

[28] W. Qiao, *Aero Acoustics of Aero Engines*, Beihang University, Beijing, China, 2010.

[29] Federal Aviation Administration, *Federal Aviation Regulation Part 36*, American Federal Aviation Press, 1993.

[30] Z. Wu, W. Qiao, S. Sun, and X. Huang, "Empirical prediction method for jet noise of aircraft engines," in *Proceedings of the Sixteenth Academic Exchange Conference of China Aviation Structural Dynamics Group*, 2008.

[31] J. Stone, C. Zola, and B. Clark, "An improved model for conventional and inverted-velocity-profile coannular jet noise," in *37th Aerospace Sciences Meeting and Exhibit*, Reno, NV, USA, 1999.

[32] J. Stone, E. Krejsa, and B. Clark, *Jet Noise Modeling for Supersonic Business Jet Application*, NASA/CR-2004-212984, 2004.

[33] J. Stone, *Interim Prediction Method for Jet Noise*, NASA-TM-X-71618, 1974.

[34] J. Stone and F. Montegani, *An Improved Prediction Method for the Noise Generated in Flight by Circular Jets*, NASA TM-81470, 1980.

[35] J. Stone, D. Groesbeck, and C. Zola, *An Improved Prediction Method for Noise Generated by Conventional Profile Coaxial Jets*, NASA-TM-82712, 1981.

[36] J. R. Stone, D. E. Groesbeck, and C. L. Zola, "Conventional profile coaxial jet noise prediction," *AIAA Journal*, vol. 21, no. 3, pp. 336–342, 1983.

[37] J. Goodykoontz and J. Stone, "Experimental study of coaxial nozzle exhaust noise," in *5th American Institute of Aeronautics and Astronautics, Aeroacoustics Conference*, Seattle, WA, USA, 1979.

[38] L. Tsague, T. T. Tatietse, J. Ngundam, and J. Tsogo, "Prediction of emissions in turbojet engines exhausts: relationship between nitrogen oxides emission index (EI_{NOx}) and the operational parameters," *Aerospace Science and Technology*, vol. 11, no. 6, pp. 459–463, 2007.

[39] P. Coen, *ARMD Strategic Thrust 2: Innovation in Commercial Supersonic Aircraft*, NASA armd-sip-thrust-2-508, 2016.

[40] A. H. Lefebvre, "Fuel effects on gas turbine combustion-liner temperature, pattern factor, and pollutant emissions," *Journal of Aircraft*, vol. 21, no. 11, pp. 887–898, 1984.

[41] N. K. Rizk and H. C. Mongia, "Semianalytical correlations for NOx, CO, and UHC emissions," *Journal of Engineering for Gas Turbines and Power*, vol. 115, no. 3, pp. 612–619, 1993.

[42] A. Dopelheuer and M. Lecht, "Influence of engine performance on emission characteristics," in *Gas Turbine Engine Combustion, Emissions and Alternative Fuels*, pp. 1–9, Lisbon, Portugal, 1999.

[43] J. J. Berton, W. J. Haller, and P. F. Senick, *A Comparative Propulsion System Analysis for the High-Speed Civil Transport*, NASA/TM-2005-213414, 2005.

[44] M. Cao, *Research on Optimization Design and Emission Analysis Method for Civil Aircraft Engine [Ph.D. thesis]*, Northwestern Polytechnical University, Xi'an, China, 2016.

[45] ICA Organization, *ICAO Aircraft Engine Emissions Databank*, ICA Organization, Germany, 2014.